Available online at www.sciencedirect.com
ScienceDirect
Archives of Biochemistry and Biophysics 459 (2007) 79–90
ABB
www.elsevier.com/locate/yabbi

Catalytic mechanism of hydride transfer between NADP$^+$/H and ferredoxin-NADP$^+$ reductase from *Anabaena* PCC 7119

Jesús Tejero [a], José Ramón Peregrina [a], Marta Martínez-Júlvez [a], Aldo Gutiérrez [b], Carlos Gómez-Moreno [a], Nigel S. Scrutton [b,1], Milagros Medina [a,*]

[a] *Departamento de Bioquímica y Biología Molecular y Celular, Facultad de Ciencias, and Institute of Biocomputation and Physics of Complex Systems (BIFI), Universidad de Zaragoza, E-50009 Zaragoza, Spain*
[b] *Department of Biochemistry, University of Leicester, University Road, Leicester LE1 7RH, UK*

Received 22 August 2006, and in revised form 20 October 2006
Available online 9 November 2006

Abstract

The mechanism of hydride transfer between *Anabaena* FNR and NADP$^+$/H was analysed using for the first time stopped-flow photodiode array detection and global analysis deconvolution. The results indicated that the initial spectral changes, occurring within the instrumental dead time upon reaction of FNR with NADP$^+$/H, included not only the initial interaction and complex formation, but also the first subsequent steps of the sequential reactions that involve hydride transfer. Two different charge-transfer complexes formed prior and upon hydride transfer, FNR$_{ox}$-NADPH and FNR$_{rd}$-NADP$^+$. Detectable amounts of FNR$_{ox}$-NADPH were found at equilibrium, but FNR$_{rd}$-NADP$^+$ accumulated to a small extent and quickly evolved. The spectral properties of both charge-transfer complexes, for the first time in *Anabaena* FNR, as well as the corresponding inter-conversion hydride transfer rates were obtained. The need of an adequate initial interaction between NADP$^+$/H and FNR, and subsequent conformational changes, was also established by studying the reactions of two FNR mutants.

Keywords: Ferredoxin-NADP$^+$ reductase; Hydride transfer; Stopped-flow; Spectra deconvolution

Ferredoxin-NADP$^+$ reductase (FNR[2], EC 1.18.1.2) is a FAD-containing enzyme that catalyses electron transfer (ET) from light reduced ferredoxin (Fd), or flavodoxin (Fld), to NADP$^+$ producing NADPH [1]. This photosynthetic role in chloroplasts and cyanobacteria vegetative cells was the first documented physiological function for this enzyme. Later, flavoproteins with FNR activity were reported in chloroplasts, phototrophic and heterotrophic bacteria, animal and yeast mitochondria and apicoplasts, demonstrating the ubiquity of FNRs among living organisms [2]. Photosynthetic FNRs show high specificity towards NADP$^+$ versus NAD$^+$ [1,3–5]. FNRs from different organisms, including *Anabaena*, have been thoroughly characterised [6–14]. Moreover, the FNR structure is the prototype of a family of flavin reductases that comprises NADPH- and NADH-dependent enzymes [15], including phthalate dioxygenase reductase [16], cytochrome b_5 reductase [17], cytochrome P450 reductase [18] or sulphite reductase [19]. All these enzymes contain a flavin-binding

* Corresponding author. Fax: +34 976 762123.
E-mail address: mmedina@unizar.es (M. Medina).
[1] Present address: Faculty of Life Sciences and Manchester Interdisciplinary Biocentre, University of Manchester, Manchester M60 1QD, UK.
[2] *Abbreviations used:* FNR, ferredoxin-NADP$^+$ reductase; FNR$_{ox}$, FNR in the fully oxidised state; FNR$_{rd}$, FNR in the hydroquinone (fully reduced) state; FNR$_{sq}$, FNR in the semiquinone state; 2′-P, 2′-phosphate group of NADP$^+$/H; ET, electron transfer; WT, wild-type; CT, charge-transfer complex; MC, Michaelis–Menten complex; Fd, ferredoxin; Fld, flavodoxin; CT-1, FNR$_{ox}$-NADPH charge-transfer complex; CT-2, FNR$_{rd}$-NADP$^+$ charge-transfer complex; 2′-P-AMP, 2′-P-AMP moiety of the NADP$^+$/H; $k_{A>B}$, $k_{B>C}$, apparent rate constants obtained by global analysis of spectral kinetic data; k_{obs}, single-wavelength detected observed rate constant; k_{HT}, k_{HT-1}, hydride transfer first-order rate constants for the direct and reverse reactions, respectively; $K_{d,NADPH}$, $K_{d,NADP^+}$, dissociation constants for the reactions of FNR reduction and oxidation, respectively.

0003-9861/$ - see front matter © 2006 Elsevier Inc. All rights reserved.
doi:10.1016/j.abb.2006.10.023

domain, which binds a molecule of either FAD or FMN, and a $NAD(P)^+/H$ binding domain and, generally operate by using reducing equivalents from the cellular NAD(P)H pool to provide low-potential electron carriers for oxidoreductive metabolisms [1,2,20].

Although the main role of FNR in photosynthetic organisms is reduction of $NADP^+$ by FNR_{rd}, this process is reversible *in vivo* and in FNRs from different sources [2]. Thus, a thorough understanding of FNR catalytic mechanism is important owing to its position as prototype for a large family of enzymes showing similar catalytic mechanisms. The mechanism of FNR reduction by NADPH has been studied [4,5,14,21–30]. In this reaction, one NADPH molecule reduces the FAD prosthetic group of the enzyme to the anionic hydroquinone state by a formal hydride transfer: $\text{E-FAD} + \text{NADPH} \rightleftharpoons \text{E-FADH}^- + \text{NADP}^+$. It is commonly accepted [2] that reduction of FNR by NADPH takes place via a two-step mechanism, in which the first observed process is related to the formation of the FNR_{ox}-NADPH (CT-1) charge-transfer complex through an intermediate Michaelis–Menten complex (MC-1), followed by hydride transfer to produce an equilibrium mixture of the CT-1 and FNR_{rd}-$NADP^+$ (CT-2) charge-transfer complexes (Scheme 1).

Observed rates for the reaction of FNR_{ox} and NADPH have been estimated to be around 800–500 s^{-1} for the first step and 200–100 s^{-1} for the second one [5,14,26,28,29,31,32]. However, since the first experimentally detected rate is faster than the accurate limit for determination with stopped-flow techniques, this model, largely derived from single-wavelength studies at 460 nm and, from studies where the spectrum was reconstructed by measurements at different wavelengths [26], might provide inadequate estimations of the rate constants and the processes related to each one. Taking into account that spectral time evolution has not been analysed in the case of the *Anabaena* FNR, that no information about evolution of CT complexes has been reported for this FNR and, that spinach and *Anabaena* FNRs although closely related show differences in the processes with $NADP^+/H$ [14], it appears appropriate to study the reaction of *Anabaena* FNR with $NADP^+/H$ on the full spectral range.

Thus, we have studied the mechanism of this reaction in *Anabaena* FNR by using stopped-flow photodiode array spectroscopic measurements for the hydride transfer and reduction of the enzyme by NADPH, as well as for the hydride transfer from FNR_{rd} to $NADP^+$. Hydride transfer mechanisms were also analysed for two FNR mutants with altered coenzyme binding properties, Tyr235Ala and Tyr235Phe [5]. The Tyr235 side-chain has been shown to stabilize $NADP^+/H$ binding through the formation of a H-bond to the 2′-P group of the coenzyme and of a stacking interaction with the adenine group (Fig. 1) [12].

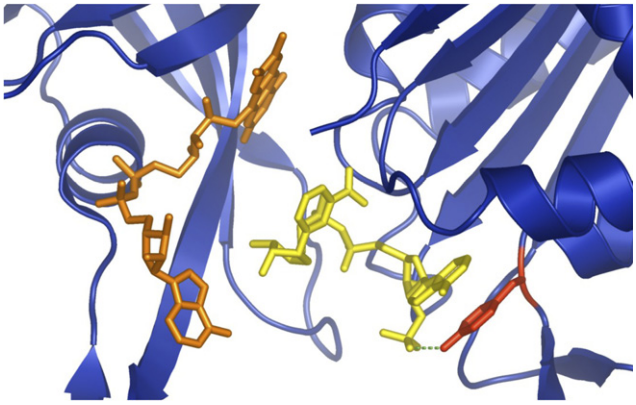

Fig. 1. Environment of the Tyr235 in the *Anabaena* FNR-$NADP^+$ complex [12]. FAD (orange), $NADP^+$ (yellow), and side-chain of Tyr235 (red) are shown as sticks. H-bond interaction between Tyr235 side-chain and the 2′-P of $NADP^+$ is indicated by a green dashed line. Produced with PyMOL [49].

Materials and methods

Site-directed mutagenesis and protein purification

The Tyr235Phe and Tyr235Ala FNR mutants were produced as described previously [5,32]. The corresponding vectors were used to transform *Escherichia coli* BL21(DE3) Gold cells (*Stratagene*). The different FNR forms were prepared from *E. coli* cultures as previously described [32,33].

Stopped-flow pre-steady-state kinetic measurements

Anaerobic fast kinetic reactions of FNR with either NADPH or $NADP^+$ were followed using an *Applied Photophysics* SF.17 MV stopped-flow contained within a customized glovebox (*Belle Technology*) (<5 ppm O_2). Under experimental conditions, instrument dead time was ~1.8 ms in single-wavelength mode and ~1.28 ms for the photodiode array detector, (for the experiments at 6 °C this instrumental dead time appears to increase up to ~3 ms). All buffers were made oxygen-free prior to introduction into the glovebox. Changes in absorbance were used to follow the reaction, either in single-wavelength mode or in a spectral range between 290 and 725 nm using a photodiode array detector. In the reactions of FNR_{rd} with $NADP^+$, 1 mM EDTA and 2 μM 5-deazariboflavin were added to the FNR solution in order to photoreduce the enzyme prior initiating the reaction. Final FNR concentrations used were 25 μM in diode array experiments and 10 μM in single-wavelength ones. A range of pyridine nucleotide concentrations were used. Multiple wavelength absorption data were collected and processed using the X-SCAN software (*Applied Photophysics Ltd.*). Typically, 400 spectra per second were collected for the processes involving WT and Tyr235Phe FNRs and 196 in the case of the Tyr235Ala FNR. Most of the experiments were carried out at 15 °C in Tris/HCl 50 mM, pH 8.0 (confirmation measurements were recorded at 6 °C). Photodiode array spectral deconvolution was performed by global analysis and numerical integration methods using Pro-K

$$\text{FNR}_{ox} + \text{NADPH} \rightleftharpoons \underbrace{\text{MC-1} \rightleftharpoons \text{CT-1}}_{\text{First step}} \rightleftharpoons \underbrace{\text{CT-2}}_{\text{Second step}} \rightleftharpoons \text{MC-2} \rightleftharpoons \text{FNR}_{rd} + \text{NADP}^+$$

Scheme 1.

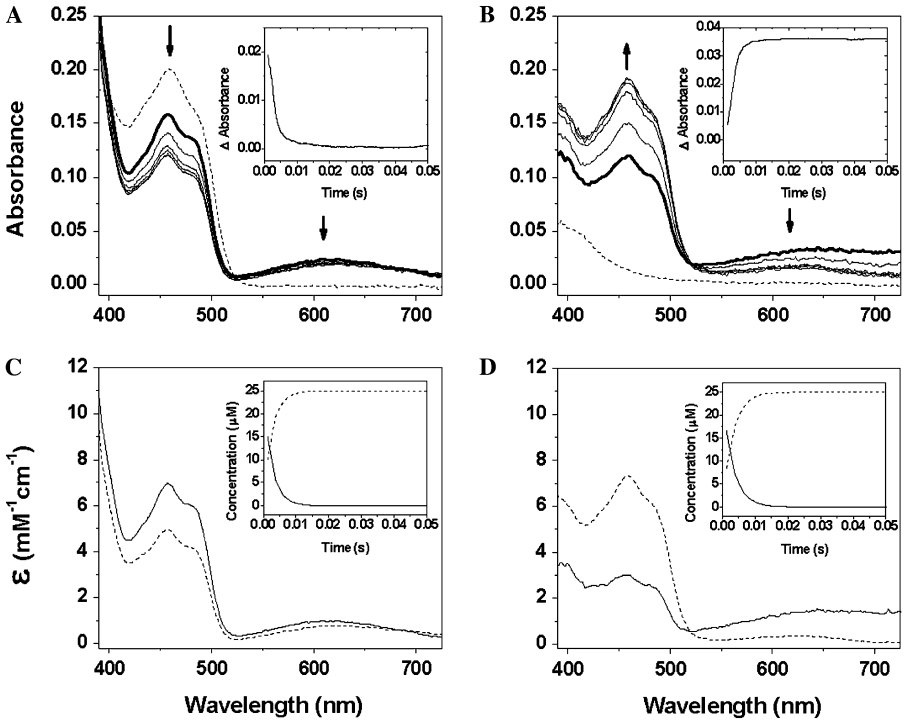

Fig. 2. Evolution of spectral changes accompanying the reactions of WT FNR with $NADP^+$/H. (A) Time course of the reaction of 25 μM WT FNR_{ox} with 250 μM NADPH and (B) 25 μM WT FNR_{rd} with 250 μM $NADP^+$ as monitored in the full spectral range. Spectra were recorded every 2.56 ms. The corresponding protein spectrum before mixing is shown as a dotted line, and the first spectrum after mixing as a bold line. Directions of absorbance changes are indicated by an arrow. Spectra after mixing are shown at 0.00128, 0.0038, 0.0064, 0.0115, 0.997 and 2.047 s. The insets show the absorption kinetic transients obtained at 458 nm with a single-wavelength detector for the reaction of 10 μM WT FNR with 100 μM $NADP^+$/H. Other experimental conditions: Tris/HCl 50 mM, pH 8.0, and 15 °C. (C and D) The absorbance spectra for the two pre-steady-state kinetically distinguishable species obtained by global analysis of the reactions in A and B, respectively. Insets show the corresponding evolution of species along the time. Species are denoted as line for the initial one (A) and a dashed line for the final (B).

software (Applied Photophysics Ltd.). Data collected over ranges from 0.00128 to 0.05 s for WT and Tyr235Phe FNRs at 15 °C, 0.0038–0.05 s for WT and Tyr235Phe FNRs at 6 °C, and up to 0.00128–8.2 s for the reactions of Tyr235Ala FNR were fit either to a single step, A > B, or to a two step, A > B > C, models (Figs. 2, 4 and 5) allowing estimation of the conversion rate constants (Table 1). A, B and C are spectral species, reflecting a distribution of enzyme intermediates at certain point along the reaction time course, and do not necessarily represent a single distinct enzyme intermediate. Moreover, none of them represents individual species of products or reactants and, their spectra can not be included as fixed values in the global-fitting. Model validity was assessed by lack of systematic deviations from residual plots at different wavelengths, inspection of calculated spectra and consistence among the number of significant singular values with the fitted model.

Estimation of K_d and k_{HT} values for the hydride transfer processes

The observed rate constants as a function of coenzyme concentration were fit to the mechanisms described in Scheme 2. Under rapid-equilibrium conditions and since the first process, formation of CT-1 or CT-2 is fast, k_{obs}, or $k_{A>B}$, values can be related with the enzyme and coenzyme concentration by [34,35]

$$k_{obs} = \frac{k_{HT\text{-}1}(K_d + [FNR] + [\ NADP^+/H]) + k_{HT}([FNR] + [NADP^+/H])}{[FNR] + [NADP^+/H] + K_d} \quad (1)$$

If concentration of coenzyme is much larger than that of the enzyme

$$k_{obs} = \frac{k_{HT\text{-}1}(K_d + [NADP^+/H]) + k_{HT}[NADP^+/H]}{[NADP^+/H] + K_d} \quad (2)$$

This simple model might apply only if the hydride transfer steps are rate-determining and the concentration of substrate is in excess over that of the enzyme. This later condition might not apply in some of our cases at the lower $NADP^+$/H concentrations used, but in some cases this can be overcome using only data obtained at ratios of $NADP^+$/H:FNR higher than 2. It should be notice that taking into account the whole system additional equilibria (Fig. 7) might be preferable. However, our data fit this equation and did not fit more complicate ones (Figs. 3A, 6A and B).

Spectral and kinetic simulations

Spectra of the intermediate CT-1 and CT-2 were estimated using the Pro-Kineticist II software (*Applied Photophysics Ltd.*) by analysis of the photodiode array data for the reaction of WT FNR_{ox} with NADPH under pseudo-first order conditions (25 μM FNR_{ox} and 250 μM NADPH). Under this conditions, the three step mechanism proposed in Scheme 3 can be used in combination with the spectra of free FNR_{ox} and FNR_{rd} forms and the kinetic constants derived from Table 2 (taking into account that for each reaction, the initial CT is formed in the instrumental dead time, indicating that kinetic rate constants for CT formation must be larger than 750 s^{-1} in the cases of WT and Tyr235Phe FNRs whatever is the direction of the initial reaction).

Time dependent spectral simulations were performed using the Pro-K software. During simulations, FNR_{ox} was considered to present a single absorbance maximum at 458 nm with a bandwidth of 20 nm and a relative height of 9.4 (extinction coefficient value), whereas FNR_{rd} was simulated by a single absorbance maximum at 380 nm with bandwidth of 50 and height of 1. CT-1 was consider with two absorbance maxima, 458 and 610 nm with bandwidths of 20 and 50 nm and, heights of 8.6 and 1.2, respectively. The corresponding parameters used for CT-2 were absor-

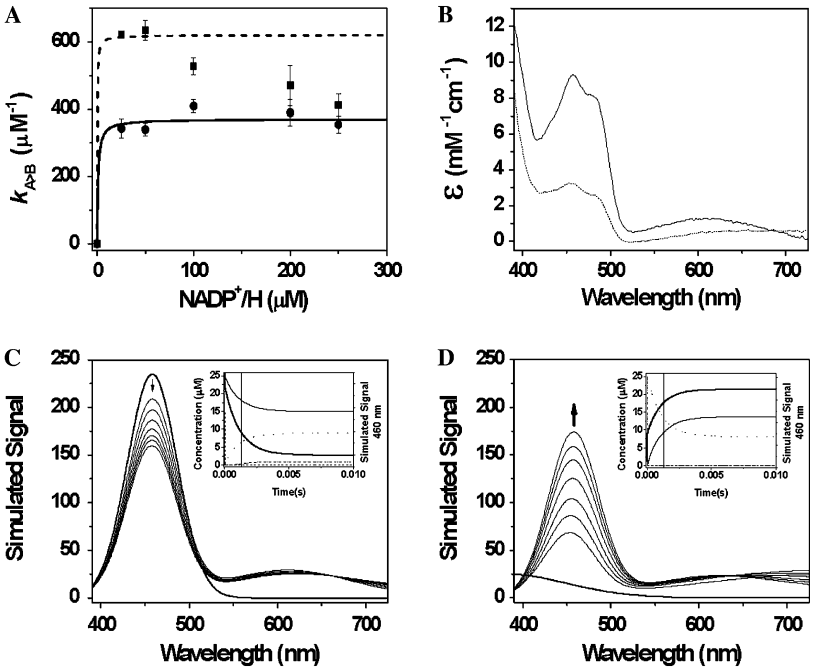

Fig. 3. (A) $k_{A>B}$ rate constants the function OF nucleotide concentration for the reactions of WT FNR_{ox} with NADPH (●) and, WT FNR_{rd} with $NADP^+$ (■). Solid and dashed lines, respectively, for NADPH and $NADP^+$, show fitting of the data to Eq. 2. (B) Spectra of CT intermediates derived by global analysis of the reaction of FNR with $NADP^+$/H; CT-1 (line) and CT-2 (dotted-line). (C) Simulation of the evolution of the reaction of WT FNR_{ox} (25 μM) with NADPH (250 μM). Spectra simulated at 0.0000, 0.0002, 0.00054, 0.0009, 0.0014, 0.002, 0.0027 and 0.01 s. (D) Simulation of the evolution of the reaction of WT FNR_{rd} (25 μM) with $NADP^+$ (250 μM). Spectra simulated at 0.0000, 0.0001, 0.00035, 0.00075, 0.0013, 0.002 and 0.01 s. The insets show evolution along the time of the different species, FNR_{ox} (dashed line), FNR_{rd} (dash-dotted line), CT-1 (line), CT-2 (dotted line) and the absorbance at 458 nm (bold line). A vertical line at the instrumental dead time indicates the part of the simulated process that must occur within the instrumental dead time (left) and the part experimentally observed (right).

bance maxima at 453 and 740 nm, bandwidths of 20 and 100 nm and heights of 3 and 1.2, respectively.

Results

Fast-kinetic processes between WT FNR and $NADP^+$/H

Reactions between WT, in oxidised or reduced states, and $NADP^+$/H were studied by stopped-flow methods using either a photodiode array detector or a single-wavelength detector at 458 nm (Figs. 2A and B). Reaction of WT FNR_{ox} with NADPH produced a long-wavelength absorbance band with a maximum around 610 nm within the experimental dead time (first spectrum after mixing at 1.28 ms, Fig. 2A). Formation of the long-wavelength absorption band occurred within the instrumental dead time at 15 °C (Fig. 2A) and 6 °C (not shown). This band was previously attributed to CT interactions between the oxidised flavin isoalloxazine ring and the nicotinamide ring of NADPH, in particular to the FNR_{ox}-NADPH charge-transfer complex (CT-1) [21,27]. Simultaneously with its formation, absorbance in the flavin band-I (459 nm) decreased within the dead time of the instrument (both at 15 and 6 °C), suggesting FNR reduction. Evolution of the flavin band-I in the following spectra indicated subsequent flavin reduction. The obtained spectra as a function of time were fitted globally by numerical integration. An A > B kinetic model was the most satisfactory in describing the absorption changes. Fig. 2C shows the species obtained by global analysis deconvolution of spectra obtained by mixing WT FNR_{ox} with NADPH (Fig. 2A). The first species observed after mixing, A, showed a spectrum consistent with the presence of FNR_{ox} and CT-1 (see Fig. 3B below), the latter being formed in the instrumental dead time and, characterised by a broad absorption band centred at 610 nm. A rapidly evolved to form species B (similar behaviour at 15 and 6 °C, despite the expected reduction in the rate constant ($k_{A>B} > 354\ s^{-1}$ at 15 °C and $>250\ s^{-1}$ at 6 °C)) (Table 1 and Fig. 2C). Comparison of species B with A indicated FNR reduction, as well as a small decrease in the intensity of the peak of the CT-1 band, which also resulted displaced to longer wavelengths. This suggested formation of a small amount of FNR_{rd}-$NADP^+$ CT (CT-2) in equilibrium with CT-1 (Fig. 2C).

When analysing the reduction of $NADP^+$ by FNR_{rd} (Fig. 2B), the first recorded spectrum after mixing (1.28 ms, bold line in Fig. 2B) showed a CT band absorbance with a maximum beyond 700 nm, consistent with CT-2 formation [26]. Similar results were observed at 15 and 6 °C and we were unable to follow the time dependent formation of this absorption band. In this spectrum, the flavin absorbance band-I showed significant oxidation of the enzyme, and the pronounced absorbance in the 500–700 nm range suggested a mixture of the FNR_{ox}-NADPH

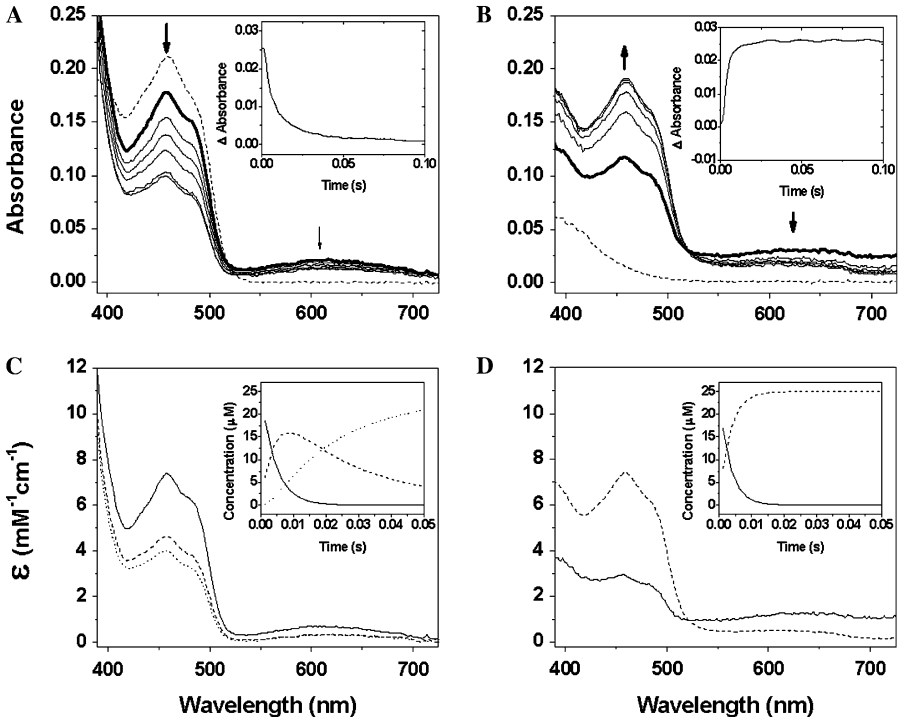

Fig. 4. Evolution of spectral changes accompanying reactions of Tyr235Phe FNR with $NADP^+$/H. (A) Time course of the reaction of 25 μM Tyr235Phe FNR_{ox} with 250 μM NADPH and (B) 25 μM Tyr235Phe FNR_{rd} with 250 μM $NADP^+$ as monitored in the full spectral range. The insets show the corresponding absorption kinetic transients obtained at 458 nm with a single-wavelength detector. Other conditions as in Fig. 2. (C and D) The absorbance spectra for the two pre-steady-state kinetically distinguishable species obtained by global-fitting analysis of reactions in A and B, respectively. Insets show the corresponding evolution of species along the time. Species are denoted as line for the initial one (A), a dashed line for the intermediate (B) and a dotted line for the final (C).

and FNR_{rd}-$NADP^+$ CTs. Spectra recorded at different times after the initial indicated further FNR oxidation, as well as evolution of CT-2 to CT-1. The final equilibrium established appeared to present some FNR_{ox} and, mainly, CT-1 as the predominant species. Again, the spectra as a function of time fitted globally to an A > B model (Fig. 2D). The spectrum for species A showed a broad band in the 600–720 nm region consistent with a mixture of CT-1 and CT-2. That this was the first spectral species obtained indicated that FNR_{rd} associated with $NADP^+$ to produce CT-2 (characterised by a maximum above 730 nm) and hydride transfer started to produce CT-1 within the instrument dead time. Species A evolved rapidly to form B ($k_{A>B} = 413\ s^{-1}$ at 15 °C and >300 s^{-1} at 6 °C) (Fig. 2D). A comparison of species B with A indicated an increase in the absorption intensity at 460 nm, consistent with almost full FNR oxidation. A decrease in the intensity CT band peak was also observed, which was also displaced to shorter wavelengths (centred at 610 nm), again consistent with the main presence of CT-1.

Since single-wavelength analysis must coincide with that of the global data analysis to confirm the mechanistic interpretations, characterisation was also performed by following the absorbance changes at 460 nm in single wavelength experiments (insets Figs. 2A and B and data at Table 1). As expected, the single wavelength absorbance transients obtained best fit to single-exponential equation and no significant improvement was achieved on fitting to a bi-exponential. The observed transients for the reactions of WT FNR recorded by single-wavelength detection showed amplitudes that corresponded to an apparent 20% reduction (inset Fig. 2A) or 30% oxidation (inset Fig. 2B) of the protein and allowed determination of k_{obs} values (Table 1). These data were in agreement with those obtained using the photodiode array detector, that present similar values for k_{obs} and which accounted for an apparent 20% reduction with NADPH and 30% oxidation with $NADP^+$ when comparing the final absorption level with that seen in the first spectrum after mixing (Figs. 2A and B). Additionally, when comparing the photodiode array time course data with the expected absorption of the fully oxidised enzyme (Fig. 2A) (or reduced, Fig. 2B) it was clear that much of the reaction had already occurred on collecting the first spectrum after mixing, and, therefore, also before the first useful point with the single-wavelength detector.

The concentration dependence of the overall rate of the process was also studied by following the above described reactions at variable concentrations of the nucleotide while keeping a constant concentration of FNR. Reactions involving WT FNR, either in the oxidised or reduced states, were mostly independent of the nucleotide concentration (Fig. 3A). Such observation was consistent with the high coenzyme affinity reported for WT FNR [27,33]. Kinetic data at much lower $NADP^+$/H concentrations or

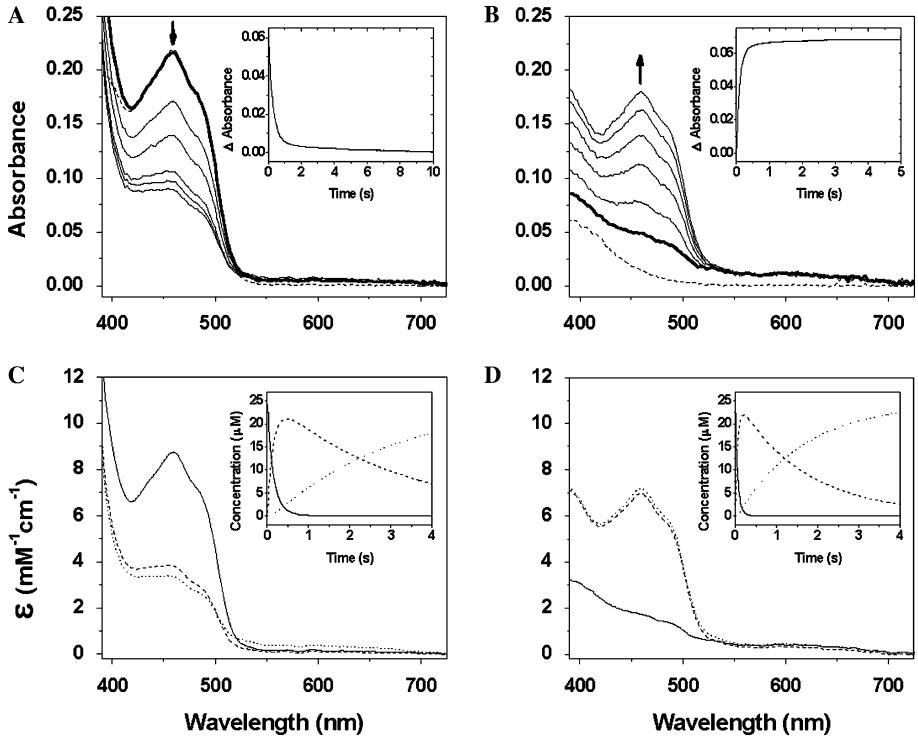

Fig. 5. Evolution of spectral changes accompanying reactions of Tyr235Ala FNR with $NADP^+$/H. (A) Time course of the reaction of 25 μM Tyr235Ala FNR_{ox} with 250 μM NADPH. Spectra after mixing are shown at 0.0038, 0.106, 0.214, 0.526, 0.997 and 4.095 s. and (B) Time course of the reaction of 25 μM Tyr235Ala FNR_{rd} with 250 μM $NADP^+$ monitored in the full spectral range. Spectra after mixing are shown at 0.0038, 0.055, 0.096, 0.178, 0.243 and 4.095 s. Spectra were recorded every 5.1 ms. The insets show the corresponding absorption kinetic transients obtained at 458 nm with a single-wavelength detector. Other conditions as in Fig. 2. (C and D) The absorbance spectra for the three pre-steady-state kinetically distinguishable species obtained by global analysis of the reactions in A and B, respectively. Insets show the corresponding evolution of species with time. Species are denoted as line for the initial one (A), a dashed line for the intermediate (B) and a dotted line for the final (C).

lower temperatures could be helpful, but in this particular case the $k_{A>B}$ and k_{obs} values under those conditions were still near the limit for the stopped-flow apparatus, as shown by the experiments recorded at 6 °C. Additionally, a slight decrease of the $k_{A>B}$ and k_{obs} values was observed upon increasing the concentration of the coenzyme. This observation correlated with that reported by Batie and Kamin [27], suggesting the presence of additional equilibria

Table 1
Kinetic rate constants obtained by stopped-flow for the reaction of FNR with $NADP^+$/H

	NADPH		$NADP^+$	
	$k_{A>B}$ (s^{-1})	$k_{B>C}$ (s^{-1})	$k_{A>B}$ (s^{-1})	$k_{B>C}$ (s^{-1})
Rate constants obtained by global analysis deconvolution of spectra obtained between 390 and 726 nm along reaction to either an A > B or an A > B > C model[a]				
WT	>354[b]	—	>413[b]	—
WT (6 °C)	>250		>300	
Y235F	178	12	309[b]	—
Y235F (6 °C)	90	5	140	
Y235A	4.8	0.4	13	0.4
	NADPH		$NADP^+$	
	k_{obs1} (s^{-1})	k_{obs2} (s^{-1})	k_{obs1} (s^{-1})	k_{obs2} (s^{-1})
Observed rate constants obtained by fitting-single-wavelength detection data at 458 nm to a single-exponential or double-exponential mechanism[c]				
WT	>430[b]	—	>469[b]	—
Y235F	151	18	260[b]	—
Y235A	3.6	0.28	9.9	0.89

Data from kinetics obtained at FNR:$NADP^+$/H ratio of 1:10 and 25 °C unless otherwise stated.

[a] Errors in the estimated values of $k_{A>B}$ and $k_{B>C}$ were ±15%.

[b] This process fits better to a single A > B model.

[c] Errors in the estimated values of k_{obs} were ±10%.

$$FNR_{ox} + NADPH \underset{}{\overset{K_{d,\ NADPH}}{\rightleftharpoons}} [FNR_{ox}\text{-}NADPH] \underset{k_{HT\text{-}1}}{\overset{k_{HT1}}{\rightleftharpoons}} [FNR_{rd}\text{-}NADP^+]$$

$$FNR_{rd} + NADP^+ \underset{}{\overset{K_{d,\ NADP+}}{\rightleftharpoons}} [FNR_{rd}\text{-}NADP^+] \underset{k_{HT1}}{\overset{k_{HT\text{-}1}}{\rightleftharpoons}} [FNR_{ox}\text{-}NADPH]$$

Scheme 2.

involving the formation of non-productive FNR_{ox}-$NADP^+$ and FNR_{rd}-NADPH complexes (see Fig. 7). This phenomenon has also been reported in other related enzymes [36].

The observed rates as a function of coenzyme concentration might fit the simplest mechanisms describing the studied processes (Scheme 2).

In Scheme 2, $K_{d,NADPH}$ and $K_{d,NADP^+}$ are the dissociation constants for either the CT-1, or CT-2, complex and k_{HT1} or k_{HT-1} the corresponding rates of hydride transfer for each direction. Since under our experimental measurements, and due to the high affinity of the WT enzyme for both coenzymes inferred from Fig. 3A, the amount of free WT FNR was much lower than that of the coenzyme and, upon avoiding the 1:1 ratio, Eq. 2 might be used as an approximation to determine K_d and k_{HT} values. However, due to the almost independent value of rate constants on nucleotide concentration, fitting of the experimental data of Fig. 3A to Eq. 2 only provided upper limit values for the dissociation constants and lower limit values for the hydride transfer rates (Table 2). The obtained values ($K_{d,NADPH} < 1$ μM and $K_{d,NADP^+} < 0.5$ μM, for the FNR_{ox}-NADPH and the FNR_{rd}-$NADP^+$ complexes, respectively) were considerably lower than the value reported for the K_d (5.7 μM) of the FNR_{ox}-$NADP^+$ complex [33], indicating that in *Anabaena* WT FNR reduction increased the affinity for the coenzyme. These results are fully consistent with those reported for the spinach enzyme [27].

Spectra of the intermediate CT-1 and CT-2 were estimated by analysis of the spectral data along the time for the reaction of WT FNR with NADPH under pseudo-first order conditions (Fig. 3B) taking into account the three step mechanism proposed in the discussion section (Scheme 3) and the kinetic constants derived from Table 2. The spectrum derived for CT-1 species presented maxima at 458 nm and 610 nm with extinction coefficients of 8.6 $mM^{-1}\,cm^{-1}$ (slightly smaller than that of free FNR_{ox}, 9.4 $mM^{-1}\,cm^{-1}$) and 1.2 $mM^{-1}\,cm^{-1}$, respectively, and a shoulder at 480 nm. Apparently, the CT-2 species was characterized by maxima at 453 nm and beyond 726 nm with extinction coefficients of 3.0 $mM^{-1}\,cm^{-1}$ and ~0.7 $mM^{-1}\,cm^{-1}$, respectively, and a shoulder at 483 nm. Properties of these CT-1 and CT-2 spectra for *Anabaena* PCC 7119 FNR were consistent with those of the equivalent complexes reported for the processes of phthalate dioxygenase reductase when reacting with NADH [37].

To validate the estimated K_d (and the kinetic constants derived from these data) and k_{HT} values (Table 2), as well as the spectral positions and relative extinction coefficients derived for CT-1 and CT-2 species, a simulation analysis was carried out. This simulation took into account the data obtained in Table 2, the estimated spectral properties of CT-1 and CT-2 (Fig. 3B) and the fact that for the reaction in both directions the initial CT was formed in the instrumental dead time. Comparison of the obtained simulated spectra as a function of time and the evolution of the different species (Figs. 3C and D) with the experimental data in Fig. 2 indicated that our model reproduced the experimental data. Comparison of simulated evolution of species and absorbance at 460 nm (insets Figs. 3C and D) with experimental absorbance changes at 460 nm (insets Figs. 2A and B) were also consistent with the assumption of some of the derived kinetic rate constants being just lower limit values, especially for those processes involving FNR_{rd} and $NADP^+$.

Fast-kinetic processes of the Tyr235Phe and Tyr235Ala Anabaena FNR mutants with $NADP^+$/H

Reduction of Tyr235Phe FNR by NADPH (Fig. 4A) showed features similar to those of WT FNR, with formation of the CT-1. However, a concomitant decay of the CT band and the flavin absorbance band-I with time were produced, which was not observed with WT FNR. Both features indicated that when reaching the equilibrium this reaction presented a larger percentage of FNR_{rd} and less CT-1. Global analysis deconvolution of spectra obtained for the reaction of Tyr235Phe with NADPH better fit an A > B > C model (Fig. 4C). The first species observed after mixing (A, similar to WT) showed a spectrum consistent with the presence of FNR_{ox} and CT-1 that evolved to form species B, this conversion being slower than for WT (Table 1 and Fig. 2C) ($k_{A>B} \sim 178\ s^{-1}$ at 15 °C and 90 s^{-1} at 6 °C). It involved reduction of FNR and, a small decrease in the intensity of the peak of the CT-1 band together with its displacement to longer wavelengths (suggesting production of a small amount of CT-2). However, B further evolved to form species C ($k_{B>C} \sim 12\ s^{-1}$), a process that, as shown by the spectra of both species, mainly involved FNR reduction without important changes in the CT band (Fig. 4C). The reaction of Tyr235Ala FNR with NADPH was a much slower process, in agreement with previous data [5], and the CT character was barely detectable (Fig. 5A). The observed spectral changes deconvoluted to produce three different species (Fig. 5C, Table 1). We inferred that species A represented FNR_{ox} and NADPH, which if bound to the enzyme did not produce a CT species and rather represented the MC-1 complex. B mainly consisted of FNR_{rd} and hardly any CT species had accumulated. Finally, species B converted to C, decreasing further the absorption of the flavin band-I and showing a very small amount of a CT interaction.

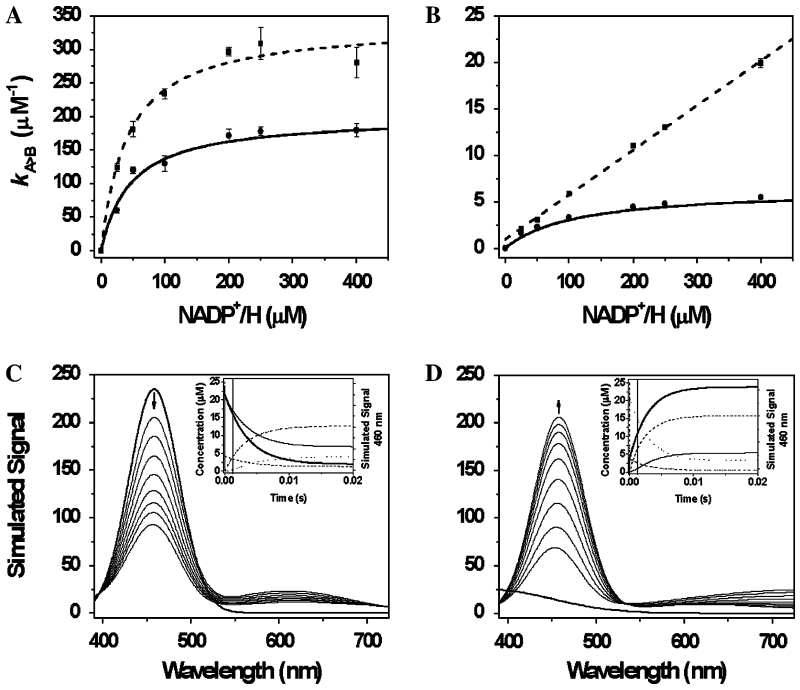

Fig. 6. $k_{A>B}$ rate constants as a function of nucleotide concentration for the reactions of (A) Tyr235Phe FNR_{rd} with $NADP^+$ (■) and Tyr235Phe FNR_{ox} with NADPH (●) and (B) Tyr235Ala FNR_{rd} with $NADP^+$ (■) and Tyr235Ala FNR_{ox} with NADPH (●). Solid and dashed lines, respectively, for NADPH and $NADP^+$, show fitting of the data to either hyperbolic (Eq. 2) or linear equations. (C) Simulation of the evolution of the reaction of Tyr235Phe FNR_{ox} (25 μM) with NADPH (250 μM). (D) Simulation of the evolution of the reaction of Tyr235Phe FNR_{rd} (25 μM) with $NADP^+$ (250 μM). Spectra shown were simulated at 0, 0.0005, 0.0012, 0.0021, 0.0032, 0.0045, 0.006, 0.008 and 0.020 s. The insets show evolution along the time of the different species, FNR_{ox} (dashed line), FNR_{rd} (dash-dotted line), CT-1 (line), CT-2 (dotted line) and the absorbance at 460 nm (bold line). A vertical line at the instrumental dead time indicates the part of the simulated process that must occur within the instrumental dead time (left) and the part experimentally observed (right).

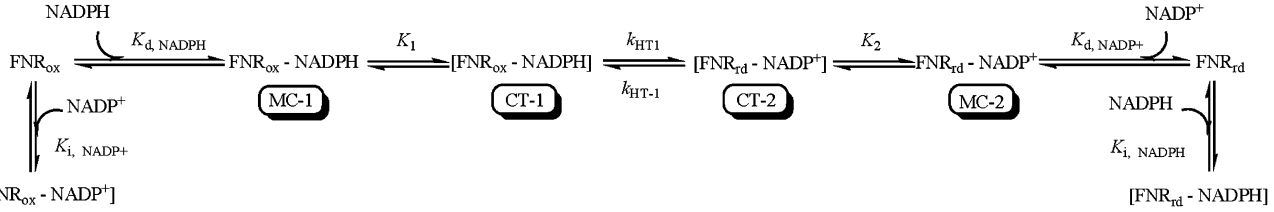

Fig. 7. Proposed mechanism for the reactions of *Anabaena* FNR with $NADP^+$/H. At high coenzyme concentrations, or by effect of mutations, the side-reactions to form the unproductive complexes FNR_{ox}-$NADP^+$ and/or FNR_{rd}-NADPH become noticeable. $K_{d,NADPH}$ and $K_{d,NADP^+}$ denote the dissociation constants for the CT-1 and CT-2 complexes, respectively. $K_{i,NADPH}$ and $K_{i,NADP^+}$ are the dissociation constants for the unproductive inhibitory complexes FNR_{rd}-NADPH and FNR_{ox}-$NADP^+$, respectively. k_{HT1} and k_{HT-1} are the hydride transfer rates for each direction.

In the reverse reaction (Fig. 4B) the Tyr235Phe mutant behaved more similarly to the WT enzyme and only a slightly smaller amount of the CT character was observed. Deconvolution of spectra obtained for this reaction fit an A > B model, with spectral features of species A and B similar to those found for the reaction of WT enzyme (Fig. 4D) and only showing a reduction in the conversion rate ($k_{A>B} = 309\ s^{-1}$ at 15 °C and $140\ s^{-1}$ at 6 °C) (Table 1). Again, reaction involving the Tyr235Ala FNR and $NADP^+$ (Figs. 5B and D) was considerably slower, and the CT character was barely detectable. The spectral data best fit a two step (three species) model (Fig. 5D, Table 1). From the deconvoluted spectral properties, we infer species A represents FNR_{rd} and $NADP^+$ (either bound (MC-2) or free) and the lack of absorbance beyond 700 nm suggested there was no formation of CT-2. B indicated formation of FNR_{ox} along with CT-1. In the conversion of species B to species C, there was a further increase in the absorption of the flavin band-I, suggesting further oxidation of FNR.

Single wavelength absorbance transients at 460 nm for processes with the Tyr235Phe and Tyr235Ala FNRs (insets Figs. 4A and B, 5A and B) were fully consistent with photodiode array data. Two observed rate constants (k_{obs1} and k_{obs2}) described the absorption changes for the reaction of Tyr235Phe with NADPH and Tyr235Ala with both redox states of the coenzyme. In all these cases, the second phase (slow, k_{obs2}) contributed only a very small change in absorption (5–7% of the total amplitude change observed, consistent with the small differences observed between spe-

Table 2
Kinetic parameters for the hydride transfer processes between FNR and $NADP^+$/H

	FNR_{ox} and NADPH		FNR_{rd} and $NADP^+$	
	$K_{d,NADPH}$ (μM^{-1})	k_{HT1} (s^{-1})	$K_{d,NADP^+}$ (μM^{-1})	k_{HT-1} (s^{-1})
Kinetic parameters derived from $k_{A>B}$ data obtained by global analysis deconvolution[a]				
WT	<1	>370	<0.2	>620
Y235F	46	200	>41	~338
Y235A	>110	6.4	—[b]	—[b]
Kinetic parameters derived from k_{obs1} values obtained at 458 nm[a]				
WT	<0.7	>501	<0.5	>560
Y235F	>60	~240	>90	~438
Y235A	>140	6.0	—[b]	—[b]

[a] Errors in the estimated values of K_d and k_{HT} values were ±20% and ±15%, respectively.
[b] Linear dependence prevented determination of these values.

cies B and C when analysing photodiode array data (Figs. 4C, 5C and D)). A single-exponential k_{obs} described the reaction between Tyr235Phe FNR_{rd} and $NADP^+$, also consistent with global analysis deconvolution (Fig. 4B). k_{obs} values, especially for Tyr235Ala, were notably slower than the ones for the WT enzyme reactions (Table 1). The amplitudes observed in single wavelength experiments for the equivalent reactions of WT and Tyr235Phe FNRs were similar (insets Figs. 2A and B, 4A and B), although, according to the diode array data (Figs. 2C and 4C), different amplitudes might be expected for the reaction with NADPH. Closer inspection of the spectra showed that reaction of WT FNR_{ox} with NADPH was completed in only 11 ms (Fig. 2A), but in the reaction of Tyr235Phe FNR_{ox} with NADPH significant reduction still took place after this time (Figs. 4A and C). Thus, the time scale used in the inset of Fig. 4A only accounted for the fast process of the reaction of Tyr235Phe FNR with NADPH. This observation agrees with the deviation observed when the kinetic traces were fit to a single-exponential equation. In reactions of Tyr235Ala FNR with either NADPH or $NADP^+$, the kinetic traces clearly fit a bi-exponential equation and the absorbance changes observed accounted for the full reactions detected in the photodiode experiments (Fig. 5, Table 1), since reactions were considerably slower than those of WT and Tyr235Phe FNRs (Table 2) and followed to their complete extent. The degree of hydride transfer achieved for each reaction was around 65%, in good agreement single-wavelength and photodiode array detected data.

Reactions of Tyr235Ala and Tyr235Phe FNR with $NADP^+$/H showed an increasing dependence of the $k_{A>B}$ and k_{obs1} values with coenzyme concentration. The $k_{A>B}$ and k_{obs1} values for the Tyr235Phe mutant suggested a hyperbolic dependence on the coenzyme concentration for both $NADP^+$ and NADPH, which almost reached saturation (Fig. 6A). The calculated $K_{d,NADPH}$ and $K_{d,NADP^+}$ values for complexes of the Tyr235Phe FNR (in the appropriate redox state) with both redox states of the coenzyme were similar between them, but two orders of magnitude larger than the values for WT (Table 2), indicating that replacement of Tyr by Phe at position 235 considerably hindered the optimal coenzyme binding to the protein. These values were lower than the value reported for the Tyr235Phe FNR_{ox}-$NADP^+$ complex ($K_d = 200\ \mu M$) [5], suggesting that, as also happens in WT FNR, reduction also increased the affinity for the coenzyme. Finally, k_{HT} and k_{HT-1} values indicated that hydride transfer was slower in this mutant than in the WT FNR (Table 2). The same simulation analysis used for the WT enzyme was used to validate the values derived for Tyr235Phe FNR in Table 2. Again, comparison of simulated (Figs. 6C and D) and experimental data (Fig. 4) validated the procedure and the obtained kinetic parameters.

Reactions involving the Tyr235Ala mutant were significantly slower. The dependence of $k_{A>B}$ and k_{obs1} on the coenzyme concentration for Tyr235Ala FNR suggested a hyperbolic dependence on NADPH concentration, whereas a linear dependence was obtained for $NADP^+$ (Fig. 6B). This is consistent with a much lower affinity for the coenzyme in this mutant than in Tyr235Phe and WT FNRs [5]. The saturation profile for the reaction between FNR_{ox} and NADPH was used to estimate limit values for K_d and k_{HT} (Table 2). The obtained values suggested a weak interaction with NADPH (consistent with the fact that previous studies did not succeed in determination of the Tyr235Ala FNR_{ox}-$NADP^+$ K_d value [5]), and a dramatic decrease in k_{HT}.

Discussion

Kinetic reaction mechanism of Anabaena FNR and $NADP^+$/H

In the reactions of *Anabaena* WT FNR with $NADP^+$/H, the photodiode array data were consistent with the formation of two CT species (Fig. 2). Their spectral features were similar to those reported for the equivalent complexes of other related flavoproteins, including FNRs [8,26,37–41]. In the reaction of WT FNR_{ox} with NADPH, formation of CT-1 as well a hydride transfer took place within the apparatus dead time. However, when reaching the equilibrium, full FNR reduction was not achieved and the spectrum of the final equilibrium mixture clearly showed the presence of CT-1 and FNR_{rd}. It should be noted that CT-2 showed little accumulation and rapidly evolved to

form CT-1 or, in less extension, FNR_{rd} plus $NADP^+$. These facts were confirmed when analysing the reverse reaction. Thus, although in the first spectrum after mixing (Fig. 2B) a considerable amount of the CT-2, in mixture with CT-1 was observed, together with a significant amount of FNR_{ox}, CT-2 rapidly evolved to CT-1 in equilibrium with FNR_{ox} plus NADPH. Global analysis of the spectra along the reaction time course clearly indicated that, in both directions, the reaction best fit an A > B model (Figs. 2C and D). Comparison of global analysis deconvolution (Table 1) and single-wavelength stopped-flow kinetic data (Table 1), clearly indicated that $k_{A>B}$ must relate to k_{obs1}. Taking all these considerations together this is, in our opinion, the simplest scheme that accounts for the experimental results here presented

where the relative length of the arrows gives and idea of the equilibrium conditions. It could be expected that Michaelis complexes (Scheme 1, Fig. 7) should be formed in each direction since, apparently, observed rate constants for CT formation are concentration independent under our experimental conditions. However, these values are close to the instrumental limit of the technique, not allowing to resolve into two sequential processes and, therefore, not relevant during the fitting.

These observations suggest that the final equilibrium species of both reactions are similar and must be closely related to the reduction potential of the enzyme [36]. This can be experimentally stated when equimolecular amounts of FNR and coenzyme react (not shown). For WT FNR it is clear that CT-2 is very unstable, rapidly decaying to CT-1 or FNR_{rd} (Fig. 2). This provides an equilibrium mixture displaced towards NADPH production, consistent with the main role of the enzyme. In the pea Tyr308Ser FNR, reduction of the enzyme in the presence of $NADP^+$ shows the formation of long-wavelength bands with an appreciable amount of CT-2, instead of CT-1 also found as predominant in the case of the WT enzyme [8]. Determination of the reduction potential of the equivalent mutant in *Anabaena* FNR showed that this variant presents a $E_{ox/rd}$ value considerably less negative than the WT enzyme [42], explaining the stabilisation of CT-2 versus the CT-1 one and supporting our interpretation of the mechanism. An analogous behaviour is observed in related proteins of the FNR family; for instance, mutant Trp1046Ala of cytochrome P450 reductase-BM3 shows a change in the redox potential with similar stabilisation of the CT-2 [41].

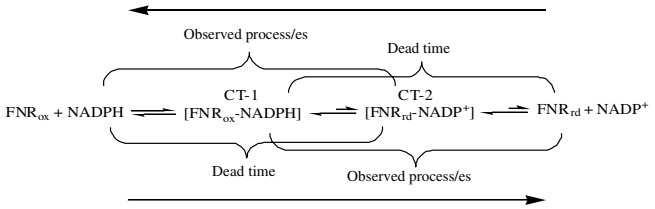

Scheme 3.

Role of Tyr235 in the formation of charge-transfer complexes in Anabaena FNR

Photodiode array stopped-flow data indicated that reaction of Tyr235Phe FNR with either NADPH or $NADP^+$ takes place through the CT-1 and CT-2 complexes observed for the WT (Fig. 4), whereas reactions of Tyr235Ala FNR with $NADP^+$/H produced insignificant amount of CT and were impaired (Fig. 5, Table 1). In both cases, although especially for the Tyr235Ala variant, weaker interactions with the coenzyme were produced (Table 2). This suggests that optimal hydride transfer requires formation of the CTs, which in the case of Tyr235Ala are difficult to form from the corresponding Michaelis–Menten complexes. The different behaviour of the Tyr235Ala FNR with respect to WT does not rule out that hydride transfer occurs after formation of CT-1, the slow rate may indicate that with this mutant the limiting step becomes the formation of CT-1 and CT-2.

Deviations from mono-exponential fits in single wavelength experiments and requirement of fitting an A > B > C model in scan mode detection are especially noticeable for the reactions of Tyr235Phe with NADPH and Tyr235Ala with either NADPH or $NADP^+$ (Figs. 4C, 5C and D), correlating the behaviour with slower reaction rates (Fig. 6, Table 1). As pointed out by Daff [36], when the lower affinity towards the coenzyme makes substrate binding (and/or the inhibitory reactions of substrate or product) increasingly important, and the hydride transfer step is no longer rate-determining, the single-exponential fit is no longer applicable. Comparison of values obtained from global analysis deconvolution with the obtained from single-wavelength stopped-flow kinetics (Table 1), shows that $k_{A>B}$ and $k_{B>C}$ might match with k_{obs1} and k_{obs2}, respectively. Therefore, mutations at position 235 allow observing how differences in the substrate binding processes modify the apparent hydride transfer rates. For mutants at position of Tyr235 hydride transfer is no longer the rate-determining step, especially in the Tyr235Ala mutant, and the decrease in stability of the produced CT complexes will determine the overall apparent rate constant. Thus, while the Tyr235Phe enzyme can still behave similarly to the WT in the reactions with the coenzyme, introduction of Ala at position 235 produces an important deleterious effect due to impairment of the interaction with $NADP^+$/H [5]. This clearly indicates that a stacking interaction between an aromatic residue of the enzyme at position 235 in *Anabaena* FNR and the adenine ring of $NAD(P)^+$/H is necessary to achieve formation of an efficient complex between the protein and the pyridine nucleotide for a subsequent hydride transfer. This is consistent with the reported mechanism indicating that initial recognition of $NADP^+$/H by FNR occurs through the 2′-P-AMP moiety of the coenzyme and the 221–239 region of the protein [12]. The final coenzyme recognition is attained when this complex rearranges allowing the nicotinamide ring to approach the isoalloxazine ring of FNR

[12]. Replacement of Tyr235 produces disruption of the initial interaction step and might prevent the subsequent conformational changes required for optimal orientation and subsequent hydride transfer. Thus, in the case of the Tyr235Ala mutation, the important decrease of affinity is even preventing formation of CT complexes between the nicotinamide and the isoalloxazine. A Tyr at 235 is much more efficient than a Phe for $NADP^+$/H binding and orientation and, but the lack of a H-bond between Tyr and the 2′-P of NADPH in the Phe mutant still allows NADPH binding and conformational changes that evolve to CT formation. However, the weaker interaction at the initial step of recognition becomes the limiting-step and slows down the subsequent induced conformational changes, producing as final result a slower hydride transfer. Our data reflect the importance of this H-bond between the Tyr-OH and the 2′-P of $NADP^+$/H, and especially of the stacking interaction between the Tyr235 ring and the 2′-P-AMP ribose.

Role of charge-transfer complexes in fast hydride transfer

Hydride transfer in systems involving flavins and pyridine nucleotides is highly dependent on the approach and co-linear orientation of the N-5 of the flavin, the hydride to be transferred and the C-4 of the nucleotide nicotinamide ring. Upon production of such approach the nicotinamide ring can partly overlay the isoalloxazine ring, producing CT interactions. However, CT complexes might not be formed if the nicotinamide ring is held in a position where it does not overlap the isoalloxazine ring, but the co-linearity for efficient hydride transfers of C, H and N is maintained. Thus, significant formation of CT complexes occurs in systems with relative slow apparent rates [37,38], whereas more efficient hydride transfers have been reported for systems in which CT formation is not detected [43]. Therefore, although CT interactions suggest close contact between the reacting rings and might indicate if the orientation for efficient hydride transfer is achieved, CT interactions are not absolutely necessary [44]. Nevertheless, CT complexes between flavoproteins and pyridine nucleotides have been reported in numerous enzymes, including systems chemically analogous to the photosynthetic FNRs [45,46]. The CT band extinctions have been related to the fraction of enzyme molecules that form the correct interaction between NADPH and FAD for hydride transfer to occur at high rates [44] and, small changes in the efficiency of the overlap between the π orbitals of the flavin and the nicotinamide have been shown to cause important changes in the hydride transfer rates [47,48]. The kinetic data here presented show a correlation between CT complex stability and fast reaction rates. Thus, impairment of coenzyme binding in the case of the Tyr235 mutants hamper CT formation and, consequently, hydride transfer rates. This observation is in agreement with that reported for the spinach Glu312Leu and Ser96Val FNR mutants, which showed no evidence of CT complex formation and no hydride exchange ability [29,31]. In the presence of saturating amounts of coenzyme it has been shown that only a very small fraction of FNR molecules contain the nicotinamide ring placed in contact to the flavin, and are therefore competent for hydride transfer, since displacement of the C-terminal Tyr from its position appears to be required for the interaction to occur [4,14]. Thus, we can expect that in the case of FNR catalytic cycle CT interactions might not be incidental to a high rate of hydride transfer. The observed CT band intensities could be related to the fraction of enzyme molecules exhibiting the proposed movement of Tyr-terminal side-chain and the correct interaction with the coenzyme for hydride transfer to occur at high rate [44]. Nevertheless, although a good agreement between CT formation and ET rates is apparent from the limited data set used here for FNR, further work must be done to prove such hypothesis.

In conclusion, our data indicate that hydride transfer between *Anabaena* FNR and $NADP^+$/H occurs through formation of two CT complexes. Spectroscopic properties for such complexes and the hydride transfer rates for inter-conversion have been estimated. However, whereas FNR_{ox}-NADPH accumulates during the reaction and at the equilibrium point, FNR_{rd}-$NADP^+$ rapidly evolves to other FNR states. Finally, the importance of FNR and $NADP^+$/H conformations and orientation during the enzyme:coenzyme interaction is shown to be critical in the case of *Anabaena* FNR formation of CT complexes, which are necessary for an efficient hydride transfer.

Acknowledgment

This work has been supported by Comisión Interministerial de Ciencia y Tecnología (CICYT, Grant BIO2003-00627 to C.G.-M. and Grant BIO2004-00279 to M.M.) and by CONSI+D (DGA, Grant P006/2000 to M.M.). J.T. was recipient of a travel award to the University of Leicester from Caja de Ahorros de la Inmaculada-Consejo Superior de Investigación y Desarrollo.

References

[1] M. Medina, C. Gómez-Moreno, Photosynth. Res. 79 (2004) 113–131.
[2] N. Carrillo, E.A. Ceccarelli, Eur. J. Biochem. 270 (2003) 1900–1915.
[3] A.K. Arakaki, E.A. Ceccarelli, N. Carrillo, FASEB J. 11 (1997) 133–140.
[4] L. Piubelli, A. Aliverti, A.K. Arakaki, N. Carrillo, E.A. Ceccarelli, P.A. Karplus, G. Zanetti, J. Biol. Chem. 275 (2000) 10472–10476.
[5] M. Medina, A. Luquita, J. Tejero, J.A. Hermoso, T. Mayoral, J. Sanz-Aparicio, K. Grever, C. Gómez-Moreno, J. Biol. Chem. 276 (2001) 11902–11912.
[6] C.M. Bruns, P.A. Karplus, J. Mol. Biol. 247 (1995) 125–145.
[7] L. Serre, F.M. Vellieux, M. Medina, C. Gómez-Moreno, J.C. Fontecilla-Camps, M. Frey, J. Mol. Biol. 263 (1996) 20–39.
[8] Z. Deng, A. Aliverti, G. Zanetti, A.K. Arakaki, J. Ottado, E.G. Orellano, N.B. Calcaterra, E.A. Ceccarelli, N. Carrillo, P.A. Karplus, Nat. Struct. Biol. 6 (1999) 847–853.
[9] A. Dorowski, A. Hofmann, C. Steegborn, M. Boicu, R. Huber, J. Biol. Chem. 276 (2001) 9253–9263.

[10] A. Aliverti, R. Faber, C.M. Finnerty, C. Ferioli, V. Pandini, A. Negri, P.A. Karplus, G. Zanetti, Biochemistry 40 (2001) 14501–14508.
[11] G. Kurisu, M. Kusunoki, E. Katoh, T. Yamazaki, K. Teshima, Y. Onda, Y. Kimata-Ariga, T. Hase, Nat. Struct. Biol. 8 (2001) 117–121.
[12] J.A. Hermoso, T. Mayoral, M. Faro, C. Gómez-Moreno, J. Sanz-Aparicio, M. Medina, J. Mol. Biol. 319 (2002) 1133–1142.
[13] R. Morales, M.-H. Charon, G. Kachalova, L. Serre, M. Medina, C. Gómez-Moreno, M. Frey, EMBO Reports 1 (2000) 271–276.
[14] J. Tejero, I. Pérez-Dorado, C. Maya, M. Martínez-Júlvez, C. Gómez-Moreno, J.A. Hermoso, M. Medina, Biochemistry 44 (2005) 13477–13490.
[15] P.A. Karplus, C.M. Bruns, J. Bioenerg. Biomembr. 26 (1994) 89–99.
[16] C.C. Correll, C.J. Batie, D.P. Ballou, M.L. Ludwig, Science 258 (1992) 1604–1610.
[17] M.C. Bewley, C.C. Marohnic, M.J. Barber, Biochemistry 40 (2001) 13574–13582.
[18] M. Wang, D.L. Roberts, R. Paschke, T.M. Shea, B.S. Masters, J.J. Kim, Proc. Natl. Acad. Sci. USA 94 (1997) 8411–8416.
[19] A. Gruez, D. Pignol, M. Zeghouf, J. Coves, M. Fontecave, J.L. Ferrer, J.C. Fontecilla-Camps, J. Mol. Biol. 299 (2000) 199–212.
[20] J.K. Hurley, R. Morales, M. Martínez-Júlvez, T.B. Brodie, M. Medina, G. Tollin, C. Gómez-Moreno, Biochim. Biophys. Acta 1554 (2002) 5–21.
[21] V. Massey, R.G. Matthews, G.P. Foust, L.G. Howell, C.H. Williams, G. Zanetti, S. Ronchi, in: H. Sund (Ed.), Pyridine Nucleotide Dependent Dehydrogenases, Springer-Verlag, Heidelberg, 1970, pp. 393–409.
[22] S. Nakamura, T. Kimura, J. Biol. Chem. 246 (1971) 6235–6241.
[23] J.J. Keirns, J.H. Wang, J. Biol. Chem. 247 (1972) 7374–7382.
[24] R. Maskiewicz, B.H.J. Bielski, Biochim. Biophys. Acta 680 (1982) 297–303.
[25] R. Masaki, S. Yoshikawa, H. Matsubara, Biochim. Biophys. Acta 700 (1982) 101–109.
[26] C.J. Batie, H. Kamin, J. Biol. Chem. 259 (1984) 11976–11985.
[27] C.J. Batie, H. Kamin, J. Biol. Chem. 261 (1986) 11214–11223.
[28] A. Aliverti, L. Piubelli, G. Zanetti, T. Lubberstedt, R.G. Herrmann, B. Curti, Biochemistry 32 (1993) 6374–6380.
[29] A. Aliverti, C.M. Bruns, V.E. Pandini, P.A. Karplus, M.A. Vanoni, B. Curti, G. Zanetti, Biochemistry 34 (1995) 8371–8379.
[30] M. Martínez-Júlvez, J.A. Hermoso, J.K. Hurley, T. Mayoral, J. Sanz-Aparicio, G. Tollin, C. Gómez-Moreno, M. Medina, Biochemistry 37 (1998) 17680–17691.
[31] A. Aliverti, Z. Deng, D. Ravasi, L. Piubelli, P.A. Karplus, G. Zanetti, J. Biol. Chem. 273 (1998) 34008–34015.
[32] J. Tejero, M. Martínez-Júlvez, T. Mayoral, A. Luquita, J. Sanz-Aparicio, J.A. Hermoso, J.K. Hurley, G. Tollin, C. Gómez-Moreno, M. Medina, J. Biol. Chem. 278 (2003) 49203–49214.
[33] M. Medina, M. Martínez-Júlvez, J.K. Hurley, G. Tollin, C. Gómez-Moreno, Biochemistry 37 (1998) 2715–2728.
[34] S. Strickland, G. Palmer, V. Massey, J. Biol. Chem. 250 (1975) 4048–4052.
[35] A. Fersht, Structure and Mechanism in Protein Science. A Guide to Enzyme Catalysis and Protein Folding, W.H. Freeman, New York, 1999.
[36] S. Daff, Biochemistry 43 (2004) 3929–3932.
[37] G.T. Gassner, D.P. Ballou, Biochemistry 34 (1995) 13460–13471.
[38] G.T. Gassner, L. Wang, C. Batie, D.P. Ballou, Biochemistry 33 (1994) 12184–12193.
[39] G.T. Gassner, D.A. Johnson, H.W. Liu, D.P. Ballou, Biochemistry 35 (1996) 7752–7761.
[40] D.W. Konas, K. Zhu, M. Sharma, K.S. Aulak, G.W. Brudvig, D.J. Stuehr, J. Biol. Chem. 279 (2004) 35412–35425.
[41] R. Neeli, O. Roitel, N.S. Scrutton, A.W. Munro, J. Biol. Chem. 280 (2005) 17634–17644.
[42] I. Nogués, J. Tejero, J.K. Hurley, D. Paladini, S. Frago, G. Tollin, S.G. Mayhew, C. Gomez-Moreno, E.A. Ceccarelli, N. Carrillo, M. Medina, Biochemistry 43 (2004) 6127–6137.
[43] V. Favaudon, J.M. Lhoste, Biochemistry 14 (1975) 4731–4738.
[44] M. Ortíz-Maldonado, B. Entsch, D.P. Ballou, Biochemistry 42 (2003) 11234–11242.
[45] I.F. Sevrioukova, T.L. Poulos, J. Biol. Chem. 277 (2002) 25831–25839.
[46] C.C. Marohnic, M.C. Bewley, M.J. Barber, Biochemistry 42 (2003) 11170–11182.
[47] G. Blankenhorn, Eur. J. Biochem. 50 (1975) 351–356.
[48] G. Blankenhorn, Biochemistry 14 (1975) 3172–3176.
[49] W.L. DeLano, The PyMOL Molecular Graphics System DeLano Scientific, San Carlos, CA, USA, 2002.